




Article

Full-Scale Design, Implementation and Testing of an Innovative Photovoltaic Cooling System (IPCoSy)

Ryan Bugeja ^{*} , Luciano Mule' Stagno  and Ioannis Niarchos 

Institute for Sustainable Energy, University of Malta, MXK 1531 Marsaxlokk, Malta

^{*} Correspondence: ryan.m.bugeja@um.edu.mt

Abstract: The field efficiency of silicon-based solar cells is dependent on various factors including temperature. An increase in temperature results in a reduced efficiency of a magnitude dependent on the solar cell's temperature coefficient. Furthermore, an increase in solar cell temperatures beyond levels specified by the manufacturer will result in a reduced lifetime and an increased probability of potential induced degradation and even failure. Researchers have created different cooling technologies to keep the solar cells' operating temperatures to a minimum. However, no cooling technology in the literature is adequate for both land and offshore PV installations. A patented Innovative Photovoltaic Cooling System (IPCoSy) is presented in this paper. Previously published results have confirmed the cooling effect and feasibility using small-scale prototypes. This paper presents the design challenges and results of the full-scale implementation. The full-scale prototypes are the same size as commercially available photovoltaic modules, making them easier to integrate in the current market. Therefore, this research presents the results of testing full-scale prototypes while addressing challenges related to structural integrity and fluid dynamics. The findings of this research showed that the positive effects of this cooling technology range from more than a 9% increase in PV electrical energy yield, and thermal efficiencies of up to 56%. Finally, the outcome of this research will contribute towards the United Nations' sustainable development goal of affordable and clean energy through direct operational efficiency improvements in PV systems, as well as the enhanced tapping of solar energy for renewable thermal energy production.



Citation: Bugeja, R.; Mule' Stagno, L.; Niarchos, I. Full-Scale Design, Implementation and Testing of an Innovative Photovoltaic Cooling System (IPCoSy). *Sustainability* **2023**, *15*, 16900. <https://doi.org/10.3390/su152416900>

Academic Editor: Nicoletta Matera

Received: 31 October 2023

Revised: 7 December 2023

Accepted: 13 December 2023

Published: 16 December 2023



Copyright: © 2023 by the authors. Licensee MDPI, Basel, Switzerland. This article is an open access article distributed under the terms and conditions of the Creative Commons Attribution (CC BY) license (<https://creativecommons.org/licenses/by/4.0/>).

Keywords: solar energy; photovoltaics; cooling technology; photovoltaic thermal; thermal energy

1. Introduction

Photovoltaic (PV) power output is dependent on the absorbed incident solar radiation by solar cells, the efficiency and temperature coefficient of the solar cell material, and the operating temperature of the photovoltaic module. Various solutions have been proposed to optimize the absorbed incident solar radiation such as through the use of tracking mechanisms and anti-reflective coatings. Similarly, materials research has advanced the efficiency and temperature coefficients of solar cells. This research presents an innovative method to decrease the operating temperature of photovoltaic modules, and, as a result, increase their efficiency. The dependence of the efficiency on temperature is given in Equation (1) [1]. Here, n_c and $n_{T_{ref}}$ are the solar cell conversion efficiencies at a particular cell temperature and at reference temperature, respectively. β_0 is the PV module's temperature coefficient (example: 0.48%/K) and $T_c - T_{ref}$ shows the temperature difference between the cell temperature and the reference temperature [1].

$$n_c = n_{T_{ref}} \left[1 - \beta_0 (T_c - T_{ref}) \right] \quad (1)$$

An increase in temperature causes an increase in electron energy in the valence band. This results in a decrease in the material's band gap since the energy gap between the conduction band and the valence band is narrowed [1]. Furthermore, this leads to higher

intrinsic carrier concentrations, which results in an increase in the dark saturation current of the p-n junction [1]. A study by Wen Cai et al. [2] showed that the temperature effect on the short circuit current of a solar cell differs for single crystalline and polycrystalline silicon. In single crystalline silicon, the short circuit current decreases with temperature due to an increase in thermal lattice vibrations, which hinders carrier mobility. Polycrystalline silicon solar cells exhibit a slight increase in short circuit current with an increase in temperature. This effect arises partly from the decreasing band gap, which results in additional lower energy photons being absorbed and converted to charge carriers. However, this effect can also be observed in single crystalline silicon, and, in both cases, it plays a minor role. The major temperature effect in polycrystalline silicon is attributed to the ratio of recombination area decreasing at a fast rate with increasing temperature. Therefore, this leads to increased carrier mobility, which translates to an increase in the short circuit current [2]. Although the short circuit current in polycrystalline silicon solar cells can increase by 0.1% per °C, the reduction in open-circuit voltage contributes to a net decrease in the maximum power that the solar cell can deliver [3]. Elevated PV operational temperatures result in a faster degradation rate, which is even higher in open-circuit conditions [4]. This is especially true in hot climates, and, in tropical environments, PV temperatures can even exceed the maximum temperature thresholds set by the manufacturer, possibly resulting in permanent damage to the PV module [5].

Hence, it is beneficial to find a solution to lower the PV operational temperature through cooling methods. This study presents an innovative back-side water-cooling system due to its various benefits both offshore and on land. The cooling system, termed IPCoSy, involves a water chamber fitted in the space conventionally available at the back of PV modules, inside the aluminium frame, as shown in Figure 1. Whenever the controlled cooling flow is initiated, the warm water inside the cooling chamber is replaced with cooler water, resulting in a drop in the PV operating temperature. Furthermore, since the cooling water remains in contact with the back of the PV module after the cooling flow is stopped, the added specific heat capacity results in the PV module taking longer to heat up. Therefore, this cooling system requires a lower pump-switching frequency resulting in less power consumption and a longer pump lifetime. This hypothesis and the cooling system feasibility were confirmed in a previous small-scale study [6]. The small-scale study concluded that IPCoSy could achieve gains in energy yield of up to 10% with a controlled water flow and up to 3% without flow. However, this study utilised small-sized PV panels that had few commercial applications. This article presents a study aimed at designing and testing commercial size prototypes addressing challenges such as structural integrity, fluid dynamics, and the optimisation of the pump power to PV power ratio. The IPCoSy designs can be commercially viable especially when coupled with other systems such as reverse osmosis plants and water heating. The designs and applications presented in this study are protected by an international patent [7].

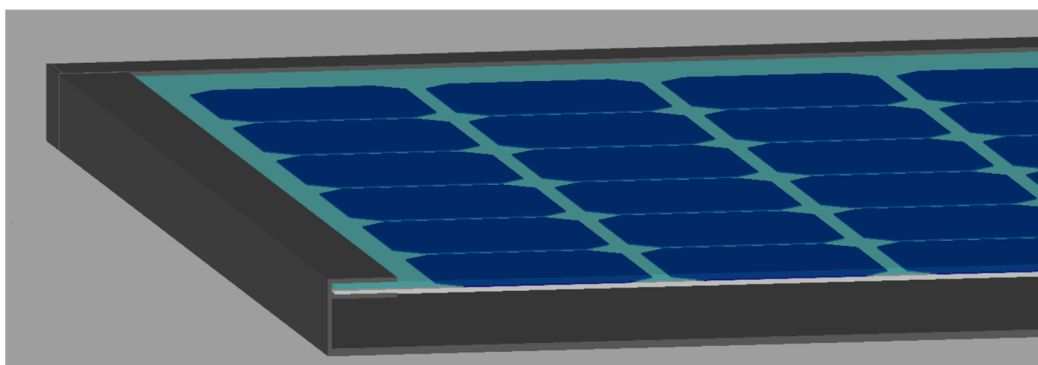


Figure 1. Cross-section showing one of the IPCoSy designs.

2. Literature and State-of-the-Art Review

The cooling of PV modules can be achieved through various methods such as forced air cooling, water cooling, thermoelectric cooling modules (TEMs), natural cooling, Phase Change Materials (PCMs), and heat sinks [3]. Passive air cooling is a cost-effective method to cool PV panels. However, the low density, thermal conductivity, and volumetric heat capacity of air result in poor thermal performance, making passive air cooling insufficient [8]. Forced (active) air cooling shows an improvement in thermal performance when compared to natural (passive) air cooling [3]. Teo et al. [9] designed an active PV air cooling system which increased solar cell operating efficiency by 3% to 6%. A well-designed PV/PCM system enables the PVs to operate in near-optimum temperatures while heating buildings at night by releasing the thermal energy stored in the PCM [10]. For a material to be adequate for use as a PCM, it must have a high thermal conductivity and a large latent heat [11]. The increase in annual energy output with the introduction of PCM with solar modules was investigated [12]. This study also identified the optimal PCM melting temperatures for different locations globally. It was found that PCM is viable mainly in places with very high insolation and little variability. Using PCM would thus increase the annual PV energy output by more than 6% in Mexico and Eastern Africa, 2–5% in Europe, and over 5% in most other locations [12]. Other systems combine PV panels, heatsinks, and TEMs [13,14]. These systems use thermoelectric modules to dissipate heat from the PV modules. Furthermore, heatsinks are used to dissipate heat from thermoelectric modules. This creates a temperature difference across the TEM, which results in the diffusion of charge carriers within the TEM materials. This results in the TEM producing power in addition to increased PV module efficiency. This setup reported a maximum decrease in PV temperature of 8.29 °C.

Water cooling is one of the most viable solutions for controlling the temperature of PV modules because of the high specific heat capacity of water. Furthermore, a water cooling technology is ideal to implement on offshore or floating PV installations due to the very large water resources available. However, when adopting a forced convection PV cooling system, one must strike a balance between increased PV efficiency due to lower temperatures and power consumed by a pump, fan, or any other device used to force convection. A study [15] determined that the ideal temperature to start cooling PVs is 45 °C, and cooling should continue until the PV module reaches a temperature of 35 °C. Water cooling can either be applied to the front or the back side of a PV module. A water film on the front side of a PV module is sometimes used to create the desired cooling effect. Furthermore, the water film helps to maintain a clean surface while also creating an anti-reflective coating, thus contributing further to an increase in solar cell operating efficiency. However, when such cooling systems are employed, one must consider power consumption by the pump and water consumption due to evaporative losses [8]. S. Nižetić et al. presented a study [16] on cooling PVs using front- and back-water spraying in a Mediterranean climate. PV temperature was reduced from 52 °C to 24 °C, with the lower temperature being limited by the temperature of the water. When considering electricity usage to pump water, a maximum of 7.7% effective increase in power output and 5.9% effective increase in efficiency were achieved. An essential improvement in this setup is eliminating the shading caused by the water sprinklers. Shading a PV module with a cooling setup may result in a power loss equal to or greater than the power gained by cooling. Furthermore, shading may cause mismatch issues on larger PV plants. Another study [17] examined the performance of a PV water pumping system with the PV module cooled by front water spraying. A maximum temperature reduction of 23 °C was achieved due to water spray and evaporative cooling. This cooling methodology increased the mean PV cell efficiency by 3.26%, and an increase in the measured short circuit current implied an improved optical performance due to the water spray on the front surface.

One of the challenges of front-side water cooling is that the water can evaporate and stain the front glass with limescale or salt if utilising seawater. Limescale build-up occurs due to the formation of calcium and magnesium carbonates. Besides being difficult to

clean, this deposit can also block some of the transmission of solar radiation to the solar cells, decreasing the efficiency of the photovoltaic module. Farrugia et al. [18] quantified the loss due to limescale build-up, which amounted to an average decrease of 2.38% in daily energy yield. Furthermore, front-side water cooling can lead to a high evaporation rate [19]. Therefore, cooling water must be replenished frequently, especially in locations where rainfall is scarce.

Various studies investigate the use of heat exchangers installed at the back of the PV module to create what is referred to as photovoltaic thermal (PVT) systems. A PVT collector consists of a PV module with fluid flowing through structures underneath the PV to absorb heat from this module [20]. The driving factor for research in PVTs is that approximately 78% of the incident solar radiation on a PV module is transformed to heat energy and not electrical energy [8]. There are two main types of PVT configurations, namely open-loop and closed-loop [21]. In an open-loop configuration, the fluid is passed once underneath the PV at a set flow rate, and the heat absorbed by the fluid is utilised instantly. An application of an open-loop PVT system is in residential direct space heating [21]. On the other hand, a closed-loop PVT system incorporates a circulating pump, which passes the fluid several times underneath the PV module to increase the amount of heat absorbed by the fluid [21]. A typical application of a closed-loop PVT system is in residential water heating. When opting to maximise PV output efficiency, open-loop PVT systems are preferred since a closed-loop system favours water heating, which would lead to the PV module reaching very high temperatures. This leads to a decrease in PV efficiency and possible delamination. A closed-loop PVT solar collector in thermosiphon mode was studied [22], achieving an electrical power enhancement of 1.56% and a thermal efficiency of 10.73%. The negligible electrical power enhancement shows that a closed-loop system does not favour PV temperature and PV electrical efficiency. Cooling channels installed at the back of PV modules can be made of various materials. However, although plastic materials are easy to use, they have poor thermal conductivity, resulting in a low heat loss coefficient. Hence, metal ducts are preferred, and, in a particular study, these yielded a heat transfer coefficient of 45.09 W/m^2 [23]. In addition to metallic ducts, this study installed a metal sheet on the back-side of the PV panel to cool the back of the PV module uniformly. Zondag et al. [24] compared four groups of combined PVT systems. The two-absorber PVT collector yielded the highest thermal efficiency of 65–66%, while the sheet and tube PVT collector yielded the highest electrical efficiency. A feasibility study by Rebollo et al. [25] gives PV module temperature and efficiency priority over hot water generation. In this study, rectangular aluminium channels were installed at the back of the PV module, resulting in a 2% increase in electrical efficiency. However, the author argues that the most significant limiting factor for heat transfer was the poor contact between the aluminium channels and the PV module. Another study [26] utilised a Solar Nor collector made from Poly(p-phenylene oxide) (PPO) plastic channels filled with ceramic granulates to cool a combination of solar cells pasted on an absorber plate. A high heat-transfer resistance was identified as one of the key factors contributing to reduced thermal efficiency compared to a conventional thermal absorber. H. Bahaidarah et al. [27] constructed a numerical model and verified it experimentally by installing a solar-thermal collector at the back of the PV module. This active cooling experiment achieved a 20% temperature drop and a 9% increase in PV panel efficiency. In another study [19], ice was also used to keep a continuous flow of water cool on the front of a PV module. This setup observed a maximum instantaneous power improvement of 24%.

Most existing cooling systems do not address the issue of a rapidly increasing PV temperature as soon as the forced cooling flow is stopped. This will lead to a high pump-switching frequency and increased power consumption, making it difficult for the cooling system to become financially viable while decreasing the lifetime of the water pump. The state-of-the-art research has a gap when it comes to finding a feasible cooling system that does not impact incident solar radiation and does not require a high pump-switching frequency, resulting in an efficient cooling flow.

3. Materials and Methods

The expected challenges when designing the full-scale prototypes were the mechanical strength of the modified PV module due to its dimensions and the internal fluid dynamics to cool the solar cells quickly and uniformly. This research aimed to obtain working full-scale prototypes that could be proposed to potential investors for further development and better manufacturability.

3.1. Prototype Design

This study focused on two main designs: a completely new photovoltaic module modified to incorporate the cooling technology, and an after-market kit that can be easily installed at the back of existing commercial PV panels to achieve a cooling effect. Throughout this article, the prototype involving the modification of a PV module and with the water in direct contact with the back sheet will be referred to as Type 1, while the after-market prototype will be referred to as Type 2. Autodesk Fusion 360 was used for the sketching of the designs and ANSYS R1 Mechanical and Fluent were used for mechanical and Computational Fluid Dynamics (CFDs) simulations, respectively.

The Type 1 prototype design involves the modification of an existing PV module to incorporate a cooling chamber at the back of the solar cell's assembly. The water inlet and outlet are placed on the back aluminium sheet on opposite corners of the PV module. A T-shaped stream spreader is installed internally at the water inlet, while two aluminium angle channels are used to stiffen the aluminium back sheet. The stiffeners have holes routed to allow water to flow through them. This prototype has a quarter-inch water inlet and a half-inch water outlet to avoid pressure build-up during cooling flows. Finally, the aluminium back sheet has another outlet to be fitted with a water-tight electrical grommet to transfer the internal junction box to a new external junction box. This enables the installation and replacement of bypass diodes. Figure 2 shows the design of the Type 1 prototype with the top removed to view internal design details.

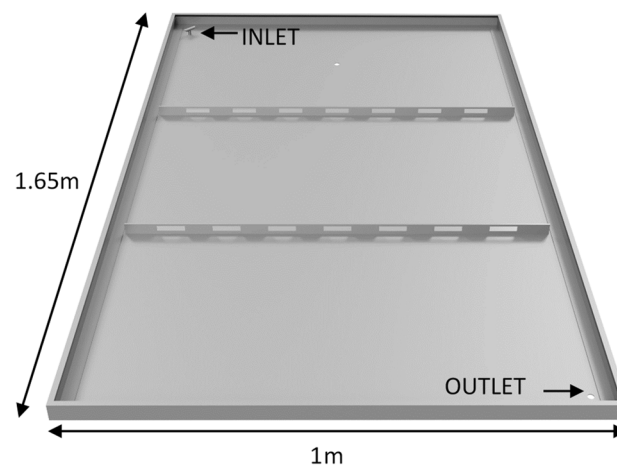


Figure 2. Design of Type 1 prototype with an open top.

The Type 2 prototype involves an aluminium tank having eight aluminium stiffeners, each alternatively attached to an opposite side of the long sides of the PV module. The stiffeners consist of solid aluminium U channels glued to the top and bottom aluminium plates. These stiffeners are used to avoid the buckling of the top aluminium plate and create a sinusoidal path for the water to flow from the inlet to the outlet. Therefore, unlike the Type 1 prototype, in the Type 2 prototype, water has to follow a specific path dictated by the stiffeners before exiting from the outlet. Inlet and outlet sizes are similar to the other prototype. However, a T-shaped stream spreader was omitted from this design since the aluminium tank is compartmentalised into smaller sections, and, therefore, controlling

the direction of the inlet water flow was unnecessary. Figure 3 shows the design of the Type 2 prototype with the top removed to view internal design details.

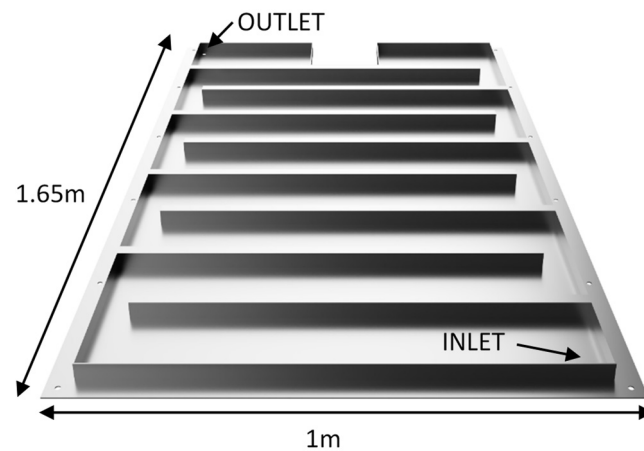


Figure 3. Design of Type 2 prototype with open top.

From the lessons learnt by designing the small-scale prototypes, it was essential to initially ensure that the seal between the bottom plate and the aluminium frame was not compromised under hydrostatic pressure. Therefore, simulations were performed to highlight the mechanical stresses and deformation resulting from hydrostatic pressures. Maximum hydrostatic pressure occurs when the module is completely filled with water and positioned vertically and in a portrait orientation. It was expected that for the Type 1 designs, both the glass and the back plate would deform under pressure; however, the extent of this deformation was unknown. The bottom plate was expected to deform considerably due to its thickness. Therefore, extra support would be needed to decrease the stress on the seal binding the plate to the aluminium frame. However, reducing the deformation of the back plate by introducing stiffeners would increase the stresses exerted on the glass, resulting in potential failure. Mechanical simulations were therefore performed to investigate ways to reduce the deformation in the glass and the aluminium back plate, without exceeding the maximum tensile strength of the solar glass.

3.2. Mechanical Simulations

The dimensions considered for the glass were 1630 mm in length, 980 mm in width, and 3.2 mm in thickness. Typically, the glass used in PV panels is toughened or pre-stressed. Toughened glass was considered, with a tensile bending strength of 120 MPa [28], Young's Modulus, E , of 73 GPa, and Poisson coefficient, ν , of 0.24. The four faces around the panel, which usually make up the PV panel's aluminium frame, were selected as fixed supports. After a mesh convergence analysis, a 10 mm mesh size was chosen. Hence, simulations were conducted to investigate the deformation and stresses on the front glass at different inclinations for both portrait and landscape installations. The results of these simulations are presented in Table 1.

Simulation shows that the glass would not fail for all landscape positions, except for in the 90° case. Hence, care must be taken during the panel installation to avoid placing it at 90° when it is full of water. Therefore, the panel must be installed at the desired inclination and filled with water afterwards. The next highest value of maximum principal stress for landscape positions is 81.24 MPa at a 30° inclination, while toughened glass theoretically fails at 120 MPa. The results in Table 1 show that all the portrait inclinations above 30° have maximum principal stresses close to the theoretical limit, with the 90° inclination exceeding this limit. This suggests that the glass could fail under hydrostatic pressure. Even if the panel does not break, the bulging of the glass could create cracks in the solar cells and affect their efficiency. Also, additional internal pressure during the filling should be avoided because of the glass's fragility. Therefore, during a cooling flow, the pressure of the piping

system must be regulated to prevent the build-up of internal pressure and risk damaging the front glass of the panels.

Table 1. Mechanical simulations of hydrostatic pressure on the front glass.

Inclination	Hydrostatic Height (mm)	Max. Deformation (mm)	Maximum Principal Stress (MPa)
Portrait			
10°	321.0	6.30	53.67
20°	597.2	7.95	83.82
30°	855.3	9.06	108.17
90°	1650	11.73	180.41
Landscape			
10°	208.1	5.14	43.07
20°	374.9	6.39	64.14
30°	530.3	7.24	81.24
90°	1000.0	9.02	124.59

The dimensions considered for the aluminium back-plate were 1580 mm in length, 930 mm in width, and 2 mm in thickness. The support stiffeners chosen were angle profiles of 25.4 mm by 25.4 mm by 3.2 mm. The material selected for the back plate and stiffeners was Aluminium 6061 T6 from the ANSYS Library. The four faces around the panel, which usually make up the PV panel's aluminium frame, were selected as fixed supports. After a mesh convergence analysis, a 7 mm mesh size was chosen. Hence, simulations were conducted to investigate the deformation of the aluminium back-plate at different inclinations for both portrait and landscape installations. The results of these simulations are presented in Table 2. Simulations at an inclination of 30° in a portrait position with three stiffeners show a deformation of 8.91 mm against 9.06 mm when two stiffeners are used. The simulation shows a deformation of 7.2 mm in the landscape position with two stiffeners and 6.27 mm with three stiffeners. Since the maximum deformation in the aluminium back-plate does not change significantly, the use of two stiffeners in the final prototype design was deemed more financially viable.

Table 2. Mechanical simulations of hydrostatic pressure on aluminium back-plate.

Number of Stiffeners	Inclination	Maximum Deformation (mm)	
		Portrait	Landscape
0	10°	7.20	6.05
	20°	8.89	7.33
	30°	10.05	8.23
	90°	12.54	10.12
2	10°	5.71	4.52
	20°	7.71	6.11
	30°	9.06	7.2
	90°	11.91	9.46
3	10°	5.24	3.49
	20°	7.45	5.12
	30°	8.91	6.26
	90°	11.92	8.63

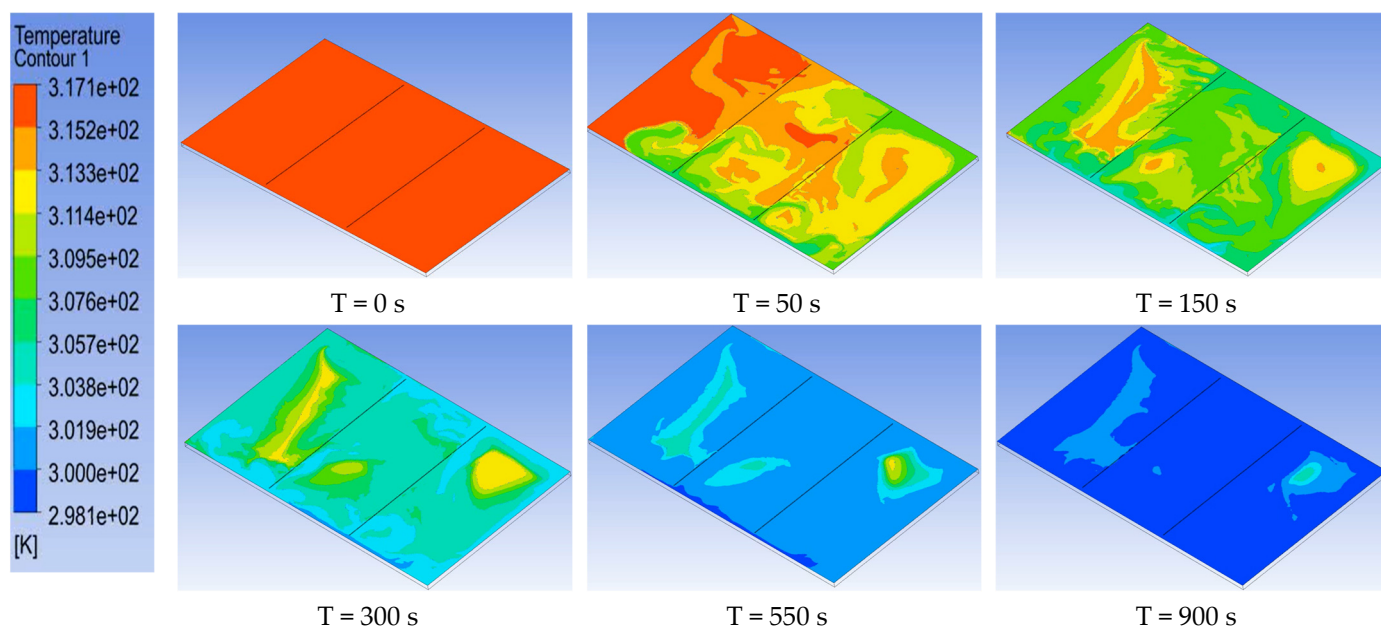
3.3. Computational Fluid Dynamic Simulations

The next step of the design was to compare both designs and analyse their effectiveness for cooling the PV module quickly and uniformly. An inlet water flow rate of 230 litres per hour (L/h) was used for the following simulations, and the simulation details are shown in Table 3.

Table 3. CFD simulation details.

Parameter	Value	
	Inlet	
Velocity Magnitude	2 m/s	
Temperature	25 °C	
	Outlet	
Gauge Pressure	0 Pa	
Backflow Total Temperature	26.85 °C	
	Inflation Layers	
Automatic Inflation	Program Controlled	
Inflation Option	Smooth Transition	
Transition Ratio	0.272	
Maximum Layers	5	
Growth Rate	1.2	

Figure 4 shows a computational fluid dynamic (CFD) simulation of the Type 1 prototype. The images shown in Figures 4 and 5 correspond to different time steps with the top images, left to right, being the first three time steps and the bottom images, left to right, corresponding to the last time steps.

**Figure 4.** CFD analysis of Type 1 prototype.

Another CFD simulation was carried out on a Type 2 prototype, as shown in Figure 5. This simulation produced results that were in line with expectations. Cool water flowed from the inlet to the outlet, pushing the hot water out and creating the desired “piston effect”. The area next to the junction box was cooled efficiently due to the lack of space between the last stiffener and the edge of the tank. This small distance allowed the entire area to be filled with cold water before exiting through the outlet.

Figure 6 plots the time taken for lowering the average temperature of the water inside Type 1 and Type 2 IPCoSy cooling systems. The Type 2 system reaches a lower average temperature quicker since the mixing of cold and hot water is limited. This, however, does not indicate a better PV cooling system since some cells are still hot while others are cool resulting in a temperature imbalance and a power output being limited by the hottest solar cells.

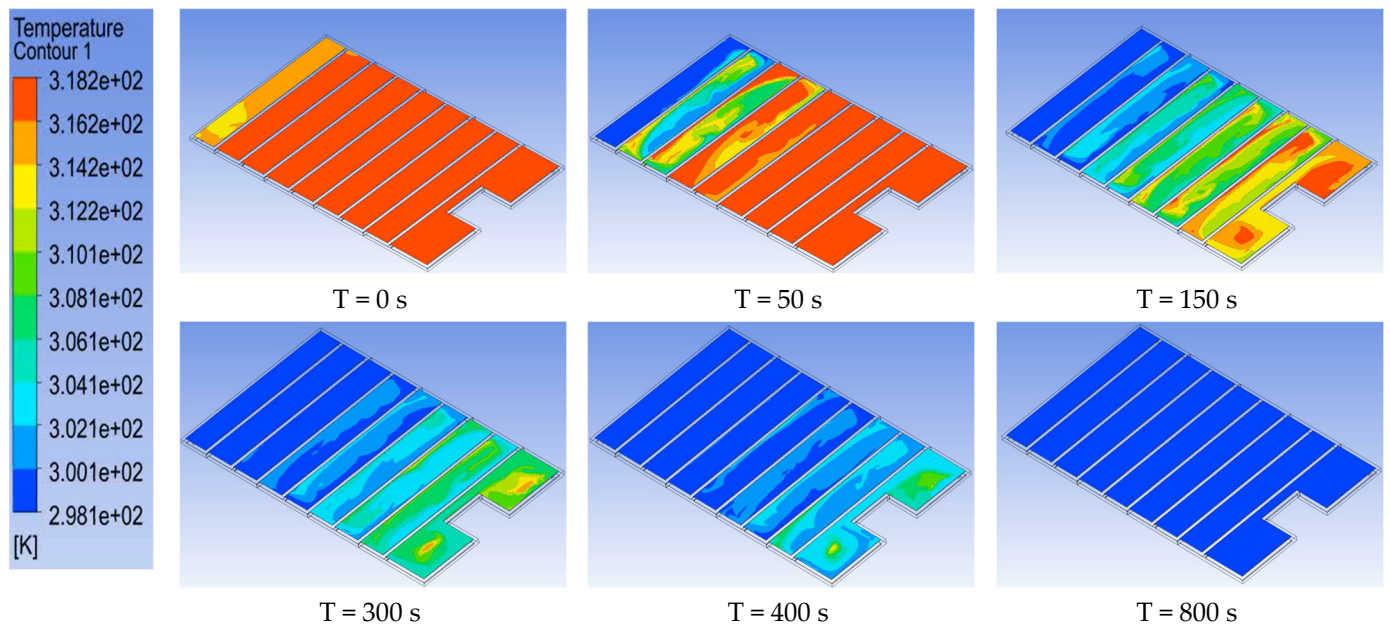


Figure 5. CFD analysis of Type 2 prototype.

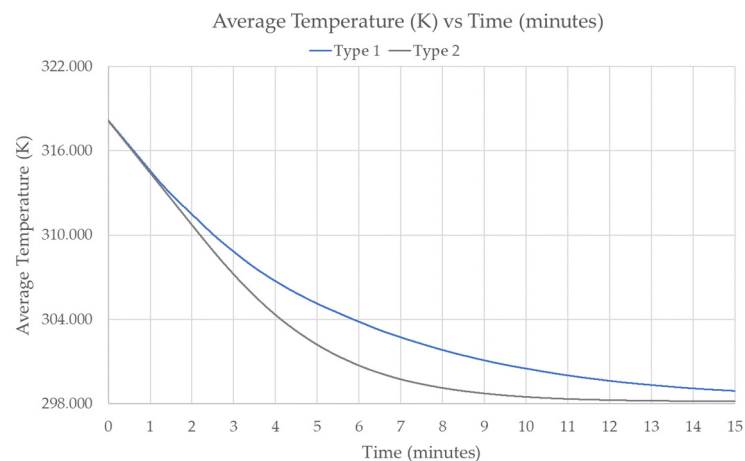


Figure 6. Average temperature (K) against time (minutes) for Type 1 and Type 2 IPCoSy cooling systems.

3.4. Experimental Setup

In the final prototypes, Type T thermocouples were attached to the back sheet of the solar cell assembly using their own glue. A thin layer of marine sealant was poured on top of the attached thermocouples to protect them from coming into direct contact with the cooling water. A type T thermocouple was chosen since, at the expected temperature ranges, these thermocouples have the highest accuracy out of all the base metal thermocouples. The predicted accuracy of Type T thermocouples is up to ± 1 °C in accordance with the standard ANSI/ASTM E230 [29]. For manufacturing the Type 2 prototypes, 3 mm aluminium sheets were cut and bent to form U channels. Some U channels were joined together to form the frame of the aluminium water tank, and the rest were used as stiffeners. A 5 mm aluminium sheet was used to close off the part of the tank that would be in contact with the back-side of the PV module, while a 3 mm back sheet was used to close off the other side of the tank. Figure 7 shows the final manufactured Type 2 prototype ready for installation.



Figure 7. IPCoSy Type 2 prototype.

Hence, an experimental setup, shown in Figure 8, was implemented to compare the different types of prototypes and to contrast a conventional PV module with IPCoSy PV modules. The setup consisted of seven ALEO X59 photovoltaic modules together with Enphase IQ7+ micro-inverters. The ALEO panels had dimensions of 1.66 m by 0.99 m with a 300 W maximum power rating at standard test conditions (STCs) and a 222 W rating at nominal conditions. The PV module had a white polymer back-sheet and 3.2 mm front toughened solar glass. Solar cells used in these panels were a type of Passivated Emitter and Rear Contact (PERC) monocrystalline silicon technology, and each module had a total of 60 solar cells. An installation angle of 10° was chosen to minimise the hydrostatic pressure on the IPCoSy modules and reduce the risk of damage during experimentation.



Figure 8. IPCoSy full-scale experimental setup.

A 300 L water tank was placed under the PV installation to be shaded from direct sunlight. A 12 V 20 W DC submersible pump was placed inside the tank to circulate water continuously through a TECO TK-2000 water chiller. The chiller was introduced to control the water supply temperature and achieve temperature stability to simulate installations where the water resource is much larger, such as in an offshore environment. The chiller power consumption will not be considered in the net energy calculations of the cooling system since this is not present in everyday scenarios. The temperature in the water tank was measured by submersing a type T thermocouple attached to an aluminium plate and sealing it to prevent water entry. A second 12 V 20 W DC submersible pump was placed inside the 300 L water tank to supply water to the IPCoSy cooling chambers when the control system switches on the cooling flow. The experimental setup consisted of two control modules, two Type 1 prototypes, two Type 2 prototypes, and a normal PV module with the back-side shielded from the cooling effect of wind. The latter module

was included to represent PV modules installed very close to the ground with limited ventilation underneath.

A Simex MultiCon CMC-141 datalogger was chosen due to its versatility in accepting various inputs by adding specific cards. A TC12 card was used to read twelve independent thermocouples with a 0.1% precision. Seven SGT-22 transmitters were used to measure AC current and convert it into a standard output signal using a Root Mean Square (RMS) value algorithm. These sensors measure current with an accuracy of 0.2% and a nonlinearity of 0.025%. The output of the seven current sensors was read by an SIAi-8 module, which can sample analogue data from up to eight devices and send these data to the datalogger through the RS-485 protocol. The SIAi-8 can sample data at an approximate frequency of 10 Hz from every channel with an accuracy of $\pm 0.25\%$.

4. Results

Prior to sending the PV panels for manufacturing and modification, the PV system was set up, including the dataloggers and sensors mentioned above, and left to operate for 55 consecutive days to obtain calibration factors. These calibration factors were essential to remove any discrepancies in the output of the PVs and inverters resulting from manufacturing tolerances. Therefore, after these calibration factors were applied to the acquired data, any discrepancies noted could be attributed to the experiment in question, which in this case would be the cooling effect.

Figure 9 represents a typical plot of temperature and power data recorded on 2 September 2022. On this day, the IPCoSy Type 2 prototype was operated with a controlled flow between 35 °C and 40 °C. In contrast the IPCoSy Type 1 prototype was filled with water and left operating without further flow. The details and results of these experiments will be presented in this section.

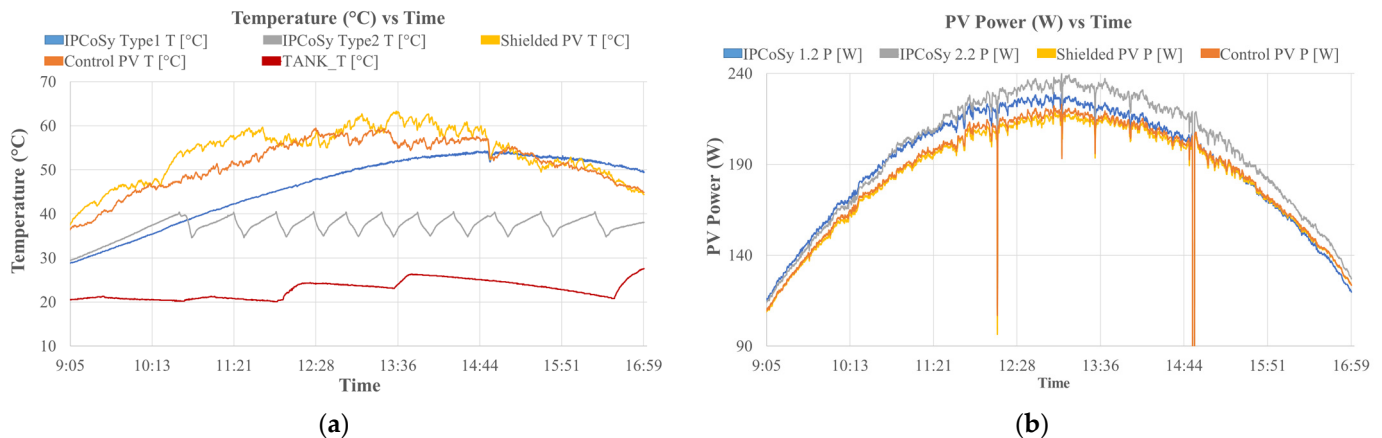


Figure 9. Recorded (a) temperature data and (b) power data for the 2 September 2022.

4.1. Testing with No Flow

In the first set of experiments, the IPCoSy prototypes were filled with water and left operating throughout the day with no flow. Power and temperature measurements were recorded throughout the no-flow experiments. Figure 10 shows the percentage gain in daily energy yield for IPCoSy Type 1 with no flow, when compared to a control PV module (a) and a back-side shielded PV module (b). Compared to the control PV module, the IPCoSy Type 1 prototype registered gains ranging from $1.15\% \pm 0.40\%$ to $3.29\% \pm 0.41\%$. In comparison, when compared to a back-side shielded PV module, the IPCoSy Type 1 prototype registered gains ranging from $1.68\% \pm 0.41\%$ to $4\% \pm 0.42\%$.

Figure 11 shows the percentage gain in daily energy yield for IPCoSy Type 2 with no flow when compared to a control PV module (a) and a back-side shielded PV module (b). Compared to the control PV module, the IPCoSy Type 2 prototype registered gains ranging from $0.60\% \pm 0.43\%$ to $0.96\% \pm 0.43\%$. In comparison, when compared to a back-side

shielded PV module, the IPCoSy 2.2 prototype registered gains ranging from $1.05\% \pm 0.43\%$ to $2.86\% \pm 0.43\%$.

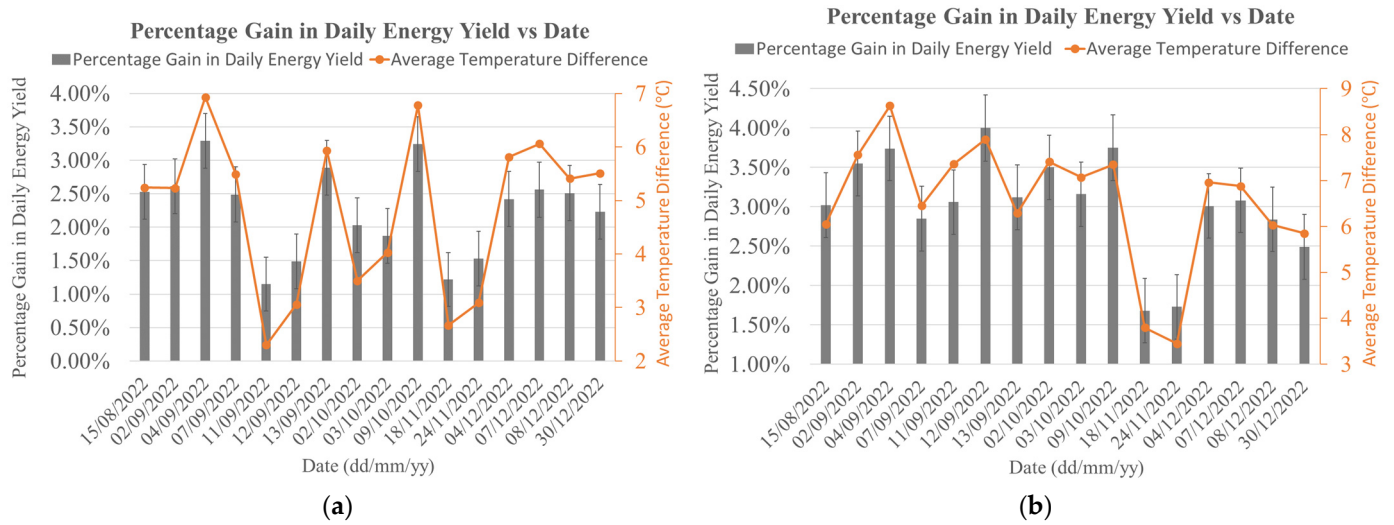


Figure 10. Percentage gain in daily energy yield for IPCoSy Type 1 with no flow when compared to a control PV module (a) and a shielded PV module (b).

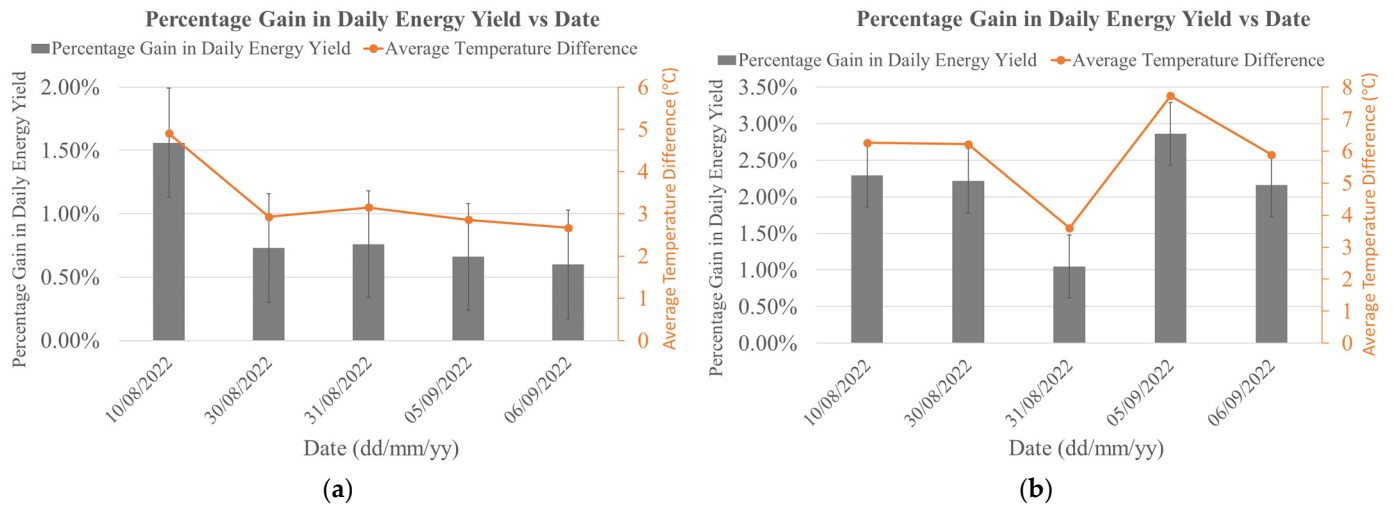


Figure 11. Percentage gain in daily energy yield for IPCoSy Type 2 with no flow when compared to a control PV module (a) and a shielded PV module (b).

An empirical temperature model was determined using the data gathered in the *No Flow* experiments. The empirical model was based on the Sandia temperature model [30] with a modification to include the time from midnight to account for the thermal inertia introduced by the high-specific-heat-capacity cooling fluid. The thermal models represented by Equations (2) and (3), respectively, show the relationship between the temperatures of the IPCoSy Type 1 and Type 2 and irradiance incident on the PV surface (G_{inc} in W/m^2), time from midnight (t in minutes), wind speed (v in m/s), and ambient temperature (T_a in $^{\circ}C$).

$$T_{IPCoSy \text{ Type 1}} = G_{inc} \times \left\{ e^{-10.0918 + (-0.0166 \times v) + (2.1946 \times \ln(t) - 8.3808)} \right\} + T_a \quad (2)$$

$$T_{IPCoSy \text{ Type 2}} = G_{inc} \times \left\{ e^{-9.6970 + (-0.1707 \times v) + (1.9686 \times \ln(t) - 6.9196)} \right\} + T_a \quad (3)$$

4.2. Testing with Controlled Flow

The results obtained from testing the large-scale prototypes with a controlled active flow are presented in this section. These experiments involved programming the control module with upper and lower temperature thresholds. Hence, the cooling flow is initiated when the IPCoSy PVs exceed the upper temperature threshold, and it is stopped when the temperature drops below the low temperature threshold. The water chamber is kept full throughout all experiments. Electrical efficiencies of PVs with no controlled flow were calculated using Equation (4), while electrical efficiencies of PVs with a controlled flow were calculated using Equation (5). In these equations, P_{out} is the PV output power (in W) and G_{inc} is the irradiance incident on the PV surface (in W/m^2). In addition, thermal efficiency was calculated using Equation (6). In this equation, M_{water} is the mass of hot water output from the system (in kg), C_{water} is the specific heat capacity of water, and $T_{out} - T_{in}$ is the difference between the average outlet water temperature and the average inlet water temperature. Finally, the combined efficiency, η_{Total} , of the PV module under test was calculated using Equation (7), where η_E is the electrical efficiency and η_{TH} is the thermal efficiency.

$$\eta_E = \frac{\text{Electrical Energy Out}}{\text{Energy In}} = \frac{\sum(P_{out} \times \text{Time})}{\sum(G_{inc} \times \text{Area} \times \text{Time})} \quad (4)$$

$$\begin{aligned} \eta_E &= \frac{\text{Electrical Energy Out} - \text{Energy consumed by Pump}}{\text{Energy In}} \\ &= \frac{\sum(P_{out} \times \text{Time}) - \sum(P_{pump} \times \text{Time})}{\sum(G_{inc} \times \text{Area} \times \text{Time})} \end{aligned} \quad (5)$$

$$\eta_{TH} = \frac{\text{Thermal Energy Out}}{\text{Energy In}} = \frac{M_{water} \times C_{water} \times (T_{out} - T_{in})}{\sum(G_{inc} \times \text{Area} \times \text{Time})} \quad (6)$$

$$\eta_{Total} = \eta_E + \eta_{TH} \quad (7)$$

Only one prototype was tested daily, while the other prototypes were filled with water and left operating with no flow to contribute to the results presented in Section 4.1 of this article. Figure 12 shows the percentage gains in energy yield by the IPCoSy Type 1 prototype compared to the control (a) and shielded (b) PV modules. The IPCoSy Type 1 prototype resulted in maximum gross and net energy gains of 7.63% and 6.78%, respectively, compared to a standard PV module installed in an open rack. Also, maximum gross and net energy gains of 9.02% and 7.64%, respectively, were recorded compared to a PV module with a wind-shielded back-side. These results were recorded with an average absolute error of $\pm 0.42\%$.

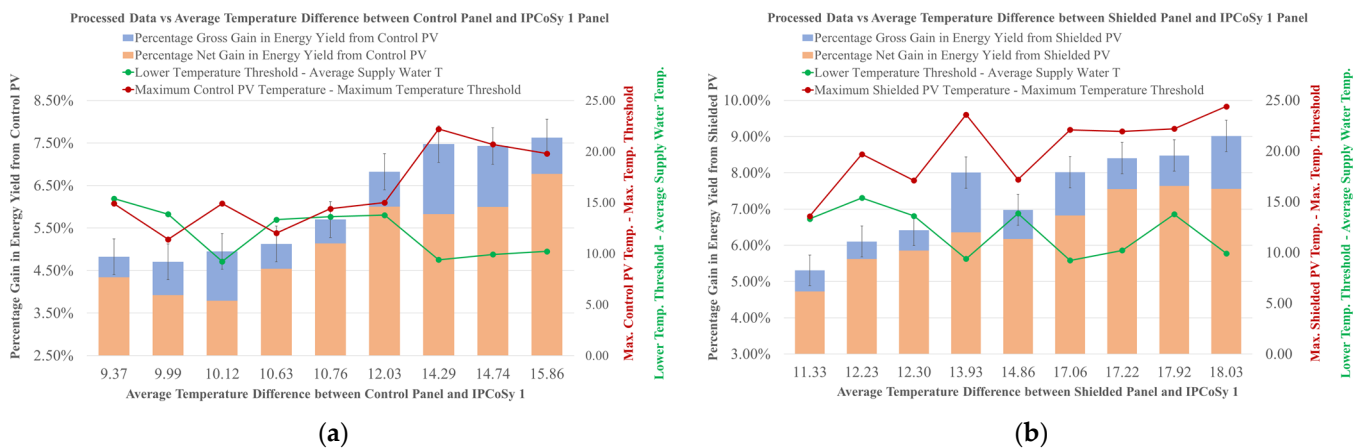


Figure 12. Plot of processed data against average temperature difference between the IPCoSy Type 1 prototype and the control PV (a) and the shielded PV (b).

The IPCoSy Type 2 module showed more structural integrity from initial testing, and no buckling was observed during cooling cycles. This robustness was expected since the top and bottom plates were attached to the central aluminium channel supports. Figure 13 shows the percentage gains in energy yield by the IPCoSy Type 2 prototype when compared to a standard PV module. Similarly, Figure 14 shows the percentage gains in energy yield by The IPCoSy Type 2 prototype when compared to a standard PV module with the back-side shielded from the effect of wind cooling. The IPCoSy Type 2 prototype resulted in maximum gross and net energy gains of 6.05% and 4.01%, respectively, compared to a standard PV module installed in an open rack. Also, maximum gross and net energy gains of 7.60% and 4.79%, respectively, were recorded compared to a PV module with a wind-shielded back-side. These results were recorded with an average absolute error of $\pm 0.42\%$.

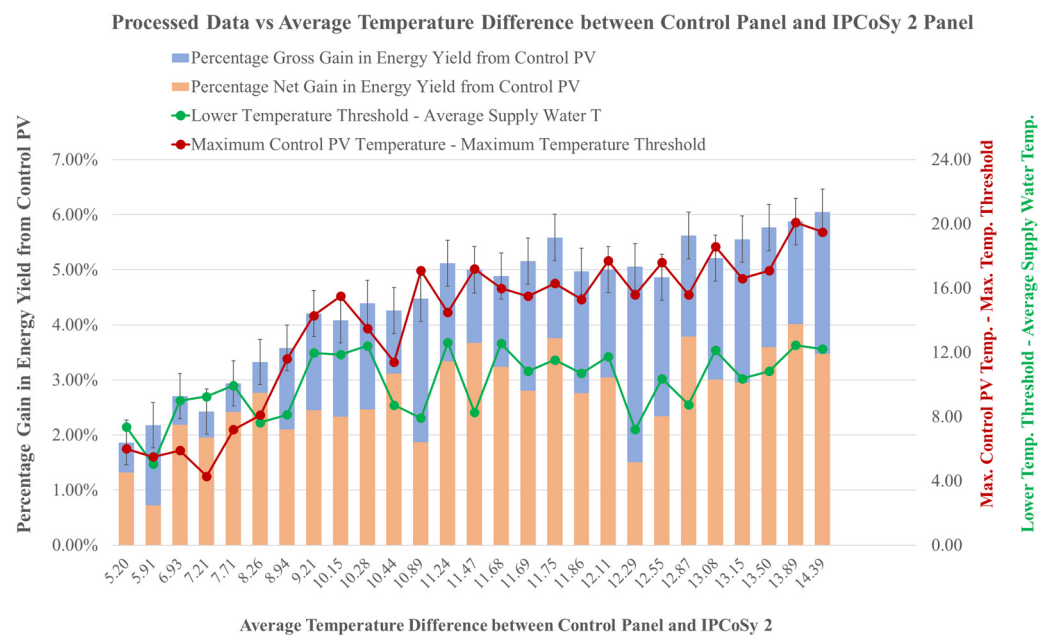


Figure 13. Plot of processed data against the average temperature difference between the control PV and the IPCoSy Type 2 prototype.

Besides the benefits of increased energy generation and lower PV maximum temperatures, the IPCoSy modules can be integrated with a water heating system to provide pre-heated water and reduce the energy consumption required. Figures 15 and 16 show a comparison of the electrical, thermal, and combined efficiencies of the PV modules under test. The colours in the legends of IPCoSy Type 1 and Type 2 correspond to the different control temperature thresholds. The IPCoSy Type 1 prototype exhibited a maximum thermal efficiency of 40.75% and a combined efficiency of 56.22%. In contrast, on the same day, the control PV module produced electrical energy at an average efficiency of 14.60%, while the shielded PV performed at an efficiency of 14.52%. In contrast, the IPCoSy Type 2 prototype exhibited a maximum thermal efficiency of 58.88% and a combined efficiency of 73.38%. On the same day, the control PV module produced electrical energy at an average efficiency of 14.01%, while the shielded PV performed at an efficiency of 13.88%. This clearly shows that the benefits of IPCoSy can increase in order of magnitude when integrated in buildings or in residential areas as part of the energy production and water heating system.

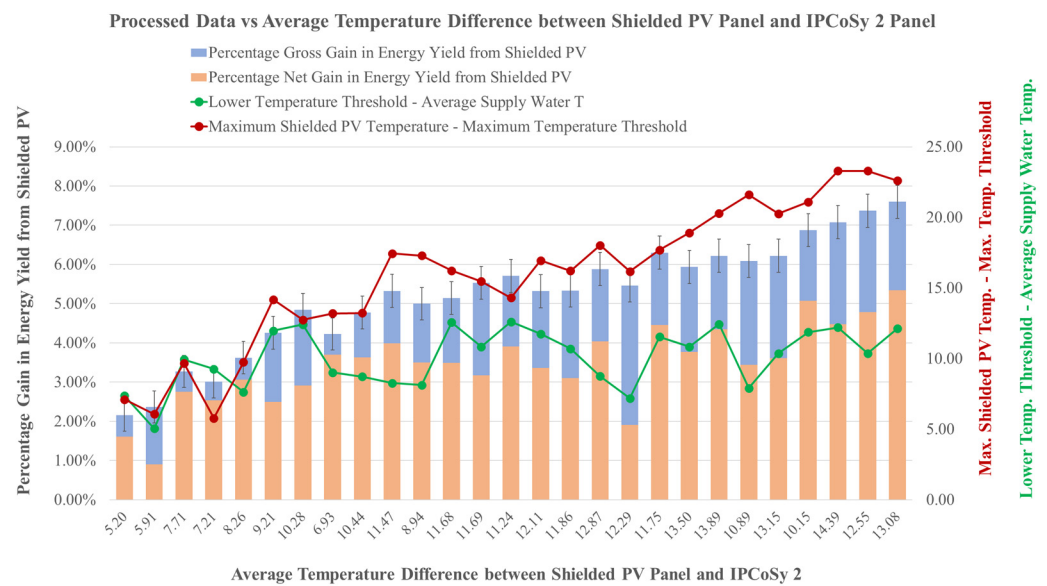


Figure 14. Plot of processed data against the average temperature difference between the shielded PV and the IPCoSy Type 2 prototype.

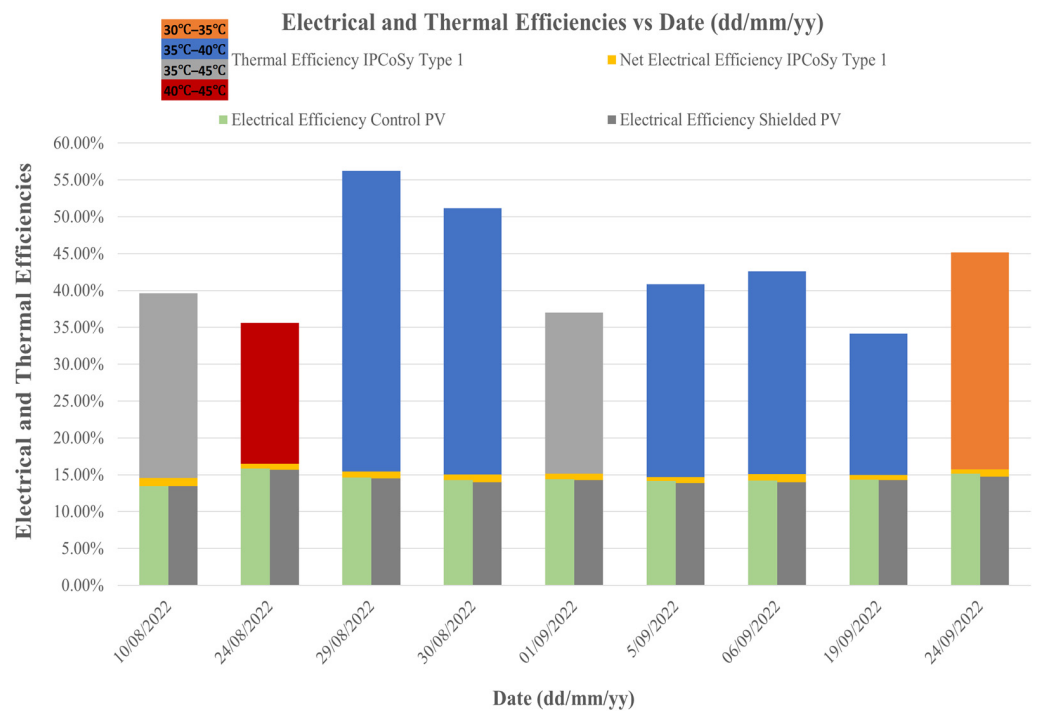


Figure 15. Electrical and thermal efficiencies on different experiment days for IPCoSy Type 1 prototype.

Throughout the large-scale experimentation, it was noted that during the summer months, temperature thresholds of 35–40 °C and 35–45 °C resulted in the highest net percentage gain in electrical energy yields, in agreement with Moharram et al. [15]. In contrast, temperature thresholds of 30–35 °C and 35–40 °C were found to increase the thermal efficiency of the IPCoSy prototype since it strikes a balance between outputting a considerable volume of water and allowing the water time to absorb enough thermal energy. Throughout experimentation, the IPCoSy Type 1 prototype outputted a 155.78 L average daily volume of hot water while the IPCoSy Type 2 outputted a 260.24 L average

daily volume of hot water. The calculations of thermal energy were based on the following assumptions and operating conditions:

- Input water temperatures were controlled by the water chiller and kept at monthly averages, as shown in Table 4.
- Output water temperatures were taken exactly at the output of the IPCoSy prototypes. Therefore, thermal losses in piping from the prototypes to the storage tank and during prolonged storage were not considered.

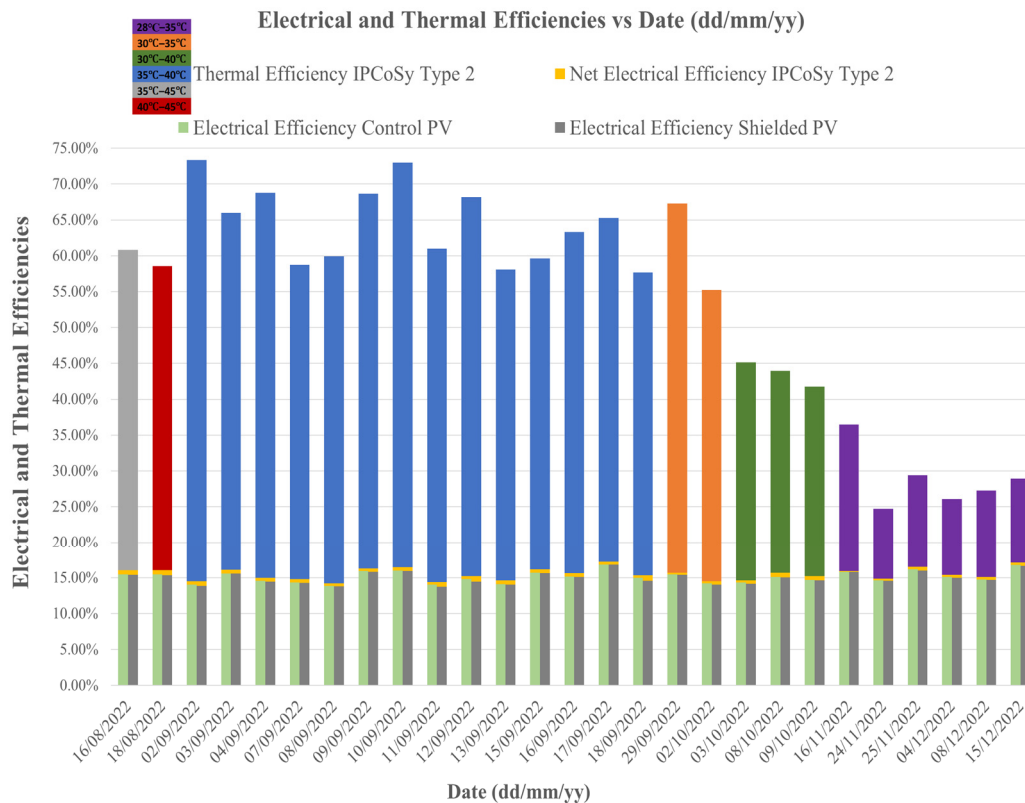


Figure 16. Electrical and thermal efficiencies on different experiment days for IPCoSy Type 2 prototype.

Table 4. Average monthly input water temperatures.

Month	Average Input Water Temperature (°C)
August	25.80
September	21.79
October	21.74
November	20.86
December	19.05

5. Discussion

This research paper presents the design, implementation, and testing of an Innovative Photovoltaic Cooling System (IPCoSy). The cooling system was tested in passive and active conditions. When no controlled flow was implemented, the energy gains of the IPCoSy Type 2 prototypes were observed to be less than the values observed for the IPCoSy Type 1 prototype. This effect could be attributed to a less efficient heat transfer between the solar cells and the cooling water due to the added aluminium sheet in contact with the PV's back sheet. Furthermore, PV modules fitted with IPCoSy Type 2 prototypes have a less efficient heat transfer to the environment since they have a double aluminium wall

with an air gap in-between and an extra 5 mm aluminium sheet in contact with the PV's back sheet. Moreover, since the cooling chamber does not cover the whole PV area due to the space allowed for the PV's junction box, there could be non-uniformities in solar cell temperatures, which result in a decreased energy gain.

The test results for cooling with a controlled flow showed that, similar to the results for the small-scale prototypes, the difference between the maximum temperature of a standard PV module and the maximum threshold temperature of the cooled PV module directly affects the percentage energy gains. Similarly, the difference between the average temperature of a standard PV module and a cooled PV module directly affects the percentage energy gains. The higher these temperature differences, the more significant the expected energy gains. Furthermore, these experimentations noted again that the difference between the lower temperature threshold and the average supply water temperature directly impacts the pump power consumption and the resulting net energy gains. The smaller this temperature difference is, the longer it will take for the IPCoSy PV to be cooled to the desired threshold. This causes the pump to work for prolonged periods, thus consuming more energy and consequently decreasing the percentage net energy gains. Another observation was that higher yields were possible when one compared an IPCoSy PV module with a standard PV module installed flat on a roof or a façade, thus blocking wind from reaching the back-side of the PV and eliminating natural and forced heat transfer. This shows that the newly designed modules are ideal for integration in buildings since it is not necessary to allow any space behind the PV modules.

It was also noted that, on average, the IPCoSy Type 2 prototype performed better than the Type 1 prototype in terms of thermal efficiency. This is because:

- The IPCoSy Type 2 prototype can dissipate less heat to the environment due to the presence of thicker aluminium sheets and double walls when fitted inside a conventional aluminium PV frame.
- The IPCoSy Type 1 prototype has a certain degree of mixing between the hot and cold water and therefore the desired low threshold temperature is reached faster, resulting in less hot water output. In contrast, as shown in Figure 5, the IPCoSy Type 2 prototype has little mixing and all the hot water has to be pushed out before the thermocouple, situated at the output of the prototype, detects the lower temperature threshold and signals the control system to stop the cooling flow. While this has a negative effect on the pump energy consumption, it results in a larger volume of water being output at a higher temperature than the input water, resulting in higher thermal efficiencies.

The IPCoSy Type 1 prototype achieves a good heat transfer between the solar cells and the cooling water. However, the structural instability makes such a prototype difficult to commercialise due to its fragility and potential for failure. Therefore, future work needs to look at ways to increase structural integrity with minimal effects on heat transfer. Another opportunity for improvement exists in the heat transfer between a conventional solar panel and IPCoSy Type 2, which is the after-market design. Researching different materials to act as a thermal interface is essential to achieving better and more uniform heat transfer. However, a compromise must be found between a material with good thermal conductivity and the maintenance of capital costs at a minimum.

An important topic that was not covered by this research is material corrosion. Since the cooling chambers will be in contact with water and even seawater, one must investigate the extent of material deterioration and its effect on the product's lifetime. Furthermore, one can research ways to mitigate this corrosion, such as by introducing changeable sacrificial materials similar to the anode rods in conventional water heaters. Finally, throughout this study, fixed water flow rates were used, and the control focused on the switching of such a flow rate. Hence, an interesting future study would simulate different flow rates and achieve the optimal flow rate that results in the highest net gains in energy production.

6. Conclusions

This paper presented the outcomes of testing a patented photovoltaic back-side cooling technology. The results showed that when a controlled flow is applied to the IPCoSy photovoltaic modules, energy gains of up to 7.63% are possible. Furthermore, this research showed that energy gains are also possible when simply filling the cooling chamber with water without any further controlled flow. Under these conditions, IPCoSy achieved energy yield gains of up to 3.29% when compared to a standard PV module installed on an open rack. When compared to a PV module installed with limited back-side ventilation, the IPCoSy module yielded 9.02% more energy when operated with controlled flow and up to 4% more energy under no flow conditions. Furthermore, IPCoSy can be coupled with existing water heating systems in order to feed water at a higher temperature. This study showed that maximum thermal efficiencies of 55.88% are possible.

These gains were possible due to the innovative features that distinguish IPCoSy from other PVT technologies. The volume of water added at the back-side of the PV module results in an increased specific heat capacity, which contributes to a delayed rise in PV temperature. Therefore, since water remains in contact with the back-side of the PV module even when controlled flow is switched off, this delayed rise in temperature results in the cooling pump switching at a lower frequency which accounts for reduced power consumption and a longer pump lifetime. IPCoSy also solves the problem of non-uniform solar cell temperatures experienced by current PVT technologies.

Finally, this paper presents the design, implementation, and testing of a product that makes the use of photovoltaic modules more sustainable through the enhanced tapping of solar energy for renewable thermal energy production. This contributes towards the United Nations' sustainable development goal of affordable and clean energy.

7. Patents

A patent titled "SYSTEM FOR COOLING A SOLAR PANEL ASSEMBLY" [7] was granted in relation to the design of the IPCoSy prototypes.

Author Contributions: Conceptualization, R.B.; methodology, R.B. and L.M.S.; simulation, I.N.; validation, R.B., L.M.S. and I.N.; formal analysis, R.B.; investigation, R.B. and I.N.; resources, L.M.S.; data curation, R.B.; writing—original draft preparation, R.B.; writing—review and editing, L.M.S. and I.N.; supervision, L.M.S.; project administration, R.B.; funding acquisition, R.B. and L.M.S. All authors have read and agreed to the published version of the manuscript.

Funding: This research was funded by the Maltese Energy and Water Agency under the National Strategy for Research and Innovation in Energy and Water (2021–2030), grant number EWA 110/20/2/002-SE.

Institutional Review Board Statement: Not Applicable.

Data Availability Statement: The data and presented in this study are available on request from the corresponding author. The data are not publicly available due to ongoing work towards a PhD award.

Acknowledgments: The authors acknowledge the administrative support of Aaron Grech, the technical support of Terence Cilia, and also Charles Yousif for providing weather data.

Conflicts of Interest: The authors declare no conflict of interest.

References

1. Chander, S.; Purohit, A.; Sharma, A.; Arvind; Nehra, S.; Dhaka, M. A study on photovoltaic parameters of mono-crystalline silicon solar cell with cell temperature. *Energy Rep.* **2015**, *1*, 104–109. [[CrossRef](#)]
2. CWen, C.; Fu, C.; Tang, J.; Liu, D.; Hu, S.; Xing, Z. The influence of environment temperatures on single crystalline and polycrystalline silicon solar cell performance. *Sci. China Phys. Mech. Astron.* **2012**, *55*, 235–241. [[CrossRef](#)]
3. Shukla, A.; Kant, K.; Sharma, A.; Biwole, P.H. Cooling methodologies of photovoltaic module for enhancing electrical efficiency: A review. *Sol. Energy Mater. Sol. Cells* **2017**, *160*, 275–286. [[CrossRef](#)]
4. Boussaid, M.; Belghachi, A.; Agroui, K.; Abdelaoui, M.; Otmani, M. Solar cell degradation under open circuit condition in out-doors-in desert region. *Results Phys.* **2016**, *6*, 837–842. [[CrossRef](#)]

5. Hasanuzzaman, M.; Malek, A.B.M.A.; Islam, M.M.; Pandey, A.K.; Rahim, N.A. Global advancement of cooling technologies for PV systems: A review. *Sol. Energy* **2016**, *137*, 25–45. [\[CrossRef\]](#)
6. Bugeja, R.; Stagno, L.M.; Niarchos, I. Photovoltaic backside cooling using the space inside a conventional frame (IPCOSY). *Future Energy* **2023**, *2*, 20–28. [\[CrossRef\]](#)
7. Bugeja, R.; Stagno, L.M. System for Cooling a Solar Panel Assembly. 285827, 24 August 2021. Available online: <https://israelpatents.justice.gov.il/en/patent-file/details/285827> (accessed on 22 June 2023).
8. Dupré, O.; Vaillon, R.; Green, M.A. *Thermal Behavior of Photovoltaic Devices*; Springer: Berlin/Heidelberg, Germany, 2017. [\[CrossRef\]](#)
9. Teo, H.G.; Lee, P.S.; Hawlader, M.N.A. An active cooling system for photovoltaic modules. *Appl. Energy* **2012**, *90*, 309–315. [\[CrossRef\]](#)
10. Huang, M.J.; Eames, P.C.; Norton, B. Thermal regulation of building-integrated photovoltaics using phase change materials. *Int. J. Heat. Mass. Transf.* **2004**, *47*, 2715–2733. [\[CrossRef\]](#)
11. Farid, M.M.; Khudhair, A.M.; Razack, S.A.K.; Al-Hallaj, S. A review on phase change energy storage: Materials and applications. *Energy Convers. Manag.* **2004**, *45*, 1597–1615. [\[CrossRef\]](#)
12. Smith, C.J.; Forster, P.M.; Crook, R. Global analysis of photovoltaic energy output enhanced by phase change material cooling. *Appl. Energy* **2014**, *126*, 21–28. [\[CrossRef\]](#)
13. Pang, W.; Liu, Y.; Shao, S.; Gao, X. Empirical study on thermal performance through separating impacts from a hybrid PV/TE system design integrating heat sink. *Int. Commun. Heat. Mass. Transf.* **2015**, *60*, 9–12. [\[CrossRef\]](#)
14. Siecker, J.; Kusakana, K.; Numbi, B.P. A review of solar photovoltaic systems cooling technologies. *Renew. Sustain. Energy Rev.* **2017**, *79*, 192–203. [\[CrossRef\]](#)
15. Moharram, K.A.; Abd-Elhady, M.S.; Kandil, H.A.; El-Sherif, H. Enhancing the performance of photovoltaic panels by water cooling. *Ain Shams Eng. J.* **2013**, *4*, 869–877. [\[CrossRef\]](#)
16. Nižetić, S.; Čoko, D.; Yadav, A.; Grubišić-Čabo, F. Water spray cooling technique applied on a photovoltaic panel: The performance response. *Energy Convers. Manag.* **2016**, *108*, 287–296. [\[CrossRef\]](#)
17. Abdolzadeh, M.; Ameri, M. Improving the effectiveness of a photovoltaic water pumping system by spraying water over the front of photovoltaic cells. *Renew. Energy* **2009**, *34*, 91–96. [\[CrossRef\]](#)
18. Farrugia, A. *Design and Analysis of Different Cooling Effects on Photovoltaic Panels*; University of Malta: Valletta, Malta, 2014.
19. Smith, M.K.; Selbak, H.; Wamser, C.C.; Day, N.U.; Krieske, M.; Sailor, D.J.; Rosenstiel, T.N. Water Cooling Method to Improve the Performance of Field-Mounted, Insulated, and Concentrating Photovoltaic Modules. *J. Sol. Energy Eng.* **2014**, *136*, 034503. [\[CrossRef\]](#)
20. Dubey, S.; Tiwari, G.N. Analysis of PV/T flat plate water collectors connected in series. *Sol. Energy* **2009**, *83*, 1485–1498. [\[CrossRef\]](#)
21. Kalogirou, S.A.; Tripanagnostopoulos, Y.; Athienitis, A. *Modeling and Simulation of Passive and Active Solar Thermal Systems*; Elsevier Ltd.: Amsterdam, The Netherlands, 2012. [\[CrossRef\]](#)
22. Arias, H.; Cabrera, J.; Hernandez, J. Performance evaluation of a mono-crystalline PV module cooled by a flat plate solar collector in thermosyphon mode. In Proceedings of the 2015 IEEE 42nd Photovoltaic Specialist Conference, PVSC, New Orleans, LA, USA, 14–19 June 2015. [\[CrossRef\]](#)
23. Arcuri, N.; Reda, F.; De Simone, M. Energy and thermo-fluid-dynamics evaluations of photovoltaic panels cooled by water and air. *Sol. Energy* **2014**, *105*, 147–156. [\[CrossRef\]](#)
24. Zondag, H.A.; de Vries, D.W.; van Helden, W.G.J.; van Zolingen, R.J.C.; van Steenhoven, A.A. The yield of different combined PV-thermal collector designs. *Sol. Energy* **2003**, *74*, 253–269. [\[CrossRef\]](#)
25. Rebollo, E.; Blanquez, F.R.; Lopez, I.; Platero, C.A.; Carrero, C. Overall feasibility of low cost conversion from PV to PVTw. In Proceedings of the 2013 International Conference on Renewable Energy Research and Applications, ICRERA, Madrid, Spain, 20–23 October 2013. [\[CrossRef\]](#)
26. Sandnes, B.; Rekstad, J. A photovoltaic/thermal (PV/T) collector with a polymer absorber plate. Experimental study and analytical model. *Sol. Energy* **2002**, *72*, 63–73. [\[CrossRef\]](#)
27. Bahaidarah, H.; Subhan, A.; Gandhidasan, P.; Rehman, S. Performance evaluation of a PV (photovoltaic) module by back surface water cooling for hot climatic conditions. *Energy* **2013**, *59*, 445–453. [\[CrossRef\]](#)
28. Purvis, I. *Handbook of Industrial Materials*, 2nd ed.; Elsevier Advanced Technology: Amsterdam, The Netherlands, 1992.
29. ASTM/ANSI E230/E230M – 17; Standard Specification for Temperature-Electromotive Force (emf) Tables for Standardized Thermocouples. ASTM International: West Conshohocken, PA, USA.
30. Fuentes, M.K. *A Simplified Thermal Model for Flat-Plate Photovoltaic Arrays*; Sandia Report; Sandia National Labs.: Albuquerque, NM, USA, 1987.

Disclaimer/Publisher’s Note: The statements, opinions and data contained in all publications are solely those of the individual author(s) and contributor(s) and not of MDPI and/or the editor(s). MDPI and/or the editor(s) disclaim responsibility for any injury to people or property resulting from any ideas, methods, instructions or products referred to in the content.